Research Article

Chao Han, Chu Cheng*, Fengling Liu, Xinli Li, Guangxin Wang, and Jiwen Li

Preparation of CdS–Ag_2S nanocomposites by ultrasound-assisted UV photolysis treatment and its visible light photocatalysis activity

https://doi.org/10.1515/ntrev-2022-0503
received August 15, 2022; accepted January 2, 2023

Abstract: Thiosulfate is a green leaching agent used in the hydrometallurgical process because it is both environmentally benign and can form the required soluble ion complexes. In this article, a novel method for the synthesis of CdS–Ag_2S nanocomposites from a solution of relevant ion complexes *via* ultrasound-assisted ultraviolet (UV) photolysis was proposed. An analysis of the mechanism revealed that the complexes undergo a series of photochemical reactions. The CdS–Ag_2S nanocomposites were synthesized by photochemical co-precipitation under UV-C irradiation. The microstructure, chemical composition, optical and electrochemical properties of the prepared nanocomposites were analyzed to verify the synthesis and investigate the product. The photodegradation of methyl orange (MO) under a xenon lamp was performed to determine the photocatalytic activity. Under visible light irradiation, the CdS–Ag_2S nanocomposites undergo the electrons transition (from valence band to conduction band) to form photogenerated electron–hole pairs realizing the effective separation of carriers and finally promote the degradation of MO to water and carbon dioxide. The subsequent degradation efficiency of the CdS–Ag_2S nanocomposites was found to be 87% after 90 min, and it was larger than 78% for pure CdS prepared *via* UV photolysis, indicating that the as-developed novel method can effectively fabricate CdS–Ag_2S photocatalyst with superior performance.

Keywords: CdS–Ag_2S nanocomposites, UV photolysis, photocatalytic activity

*** Corresponding author: Chu Cheng,** School of Materials Science and Engineering, Henan University of Science and Technology. No. 263 Kaiyuan Avenue, Luolong District, Luoyang 471023, Henan Province, China; Provincial and Ministerial Co-construction of Collaborative Innovation Center for Non-ferrous Metal New Materials and Advanced Processing Technology, Luoyang, Henan Province, China, e-mail: cheng_chu_love@126.com
Chao Han: School of Materials Science and Engineering, Henan University of Science and Technology. No. 263 Kaiyuan Avenue, Luolong District, Luoyang 471023, Henan Province, China; Provincial and Ministerial Co-construction of Collaborative Innovation Center for Non-ferrous Metal New Materials and Advanced Processing Technology, Luoyang, Henan Province, China; Research Center for High Purity Materials, Henan University of Science and Technology, Luoyang, Henan Province, China, e-mail: hanchao_0531@126.com
Fengling Liu, Xinli Li, Jiwen Li: School of Materials Science and Engineering, Henan University of Science and Technology. No. 263 Kaiyuan Avenue, Luolong District, Luoyang 471023, Henan Province, China
Guangxin Wang: Research Center for High Purity Materials, Henan University of Science and Technology, Luoyang, Henan Province, China

1 Introduction

Environmental pollution and depleting energy resources have emerged as widespread concerns because of rapid industrialization [1,2]. To effectively solve these key problems, researchers have proposed the use of new solar-driven photocatalytic materials. For example, Mukhopadhyay [3] successfully synthesized $CaFe_2O_4$ nanoparticles by a chemical precipitation technique and applied them in the degradation of brilliant green (BG) dye. Bose [4] fabricated the magnetic $MgFe_2O_4$ nanoparticles *via* a facile co-precipitation technique. Tripathy [5] used carbon-doped zinc oxide nanoparticles as a catalyst for the degradation of BG dye. Liexiao [6] adopted a one-step hydrothermal route to synthesize an interesting type of $Bi_2O_2CO_3$ hierarchical nanotubes. In particular, cadmium sulfide has been widely studied by scientists for this purpose owing to its low price, simple preparation method, and suitable band gap (2.4 eV) [7,8]. However, high photo-generated carrier recombination, poor conductivity, and significant photo-corrosion problems restrict its use in large-scale practical applications [9]. Well-known CdS-containing nanocomposites, such as CdS/MoS_2, $CdS/Bi_4V_2O_{11}$, CdS/Cu2xSe, and $CdS/Bi_4Ti_3O_{12}$, have been constructed to address these issues [10–13]. Furthermore, silver compounds, such as $AgPO_4$, AgCl, AgBr, AgI, and $AgVO_4$, with very high photocatalytic activity

have been used to create excellent photocatalytic systems utilizing these CdS nanocomposites [14,15]. Ag_2S, which possesses a bandgap range of 0.9–1.0 eV, is a semiconductor (n-type) with a distinctive structure and good physical properties. Additionally, owing to its excellent photoelectric properties, doping with Ag_2S is an effective strategy for enhancing the photocatalytic activity of CdS-supported catalysis because it lowers the photo-generated carrier recombination rate and reduces photo-corrosion. According to numerous reports, combining Ag_2S with CdS semiconductors can increase the overall photocatalytic activity. As a result, the synthesis of Ag_2S and CdS has recently received significant research attention [16–19].

The most widely used method for preparing a CdS–Ag_2S nanocomposite photocatalyst preparation is to load Ag_2S onto CdS carriers *via* deposition precipitation. However, during the preparation process, Ag_2S will self-nucleate, preventing close contact between Ag_2S and CdS, thereby hindering the transmission of photogenerated carriers to a certain extent. Several methods have been applied in Ag_2S and CdS preparation, such as ion implantation, thermal evaporation technique, and sol–gel methods [20,21]. Among them, the chemical co-precipitation method is an effective and time-efficient method to obtain Ag_2S and CdS nanoparticles. As a result, most researchers employ the chemical co-precipitation method with various chemical reagents and conditions to synthesize these nanoparticles. Based on previous studies, this study proposes a novel photochemical co-precipitation method to obtain these nanocomposites. In this proposed method, thiosulfate has been used as a green chemical reagent for the metallurgical leaching of cadmium and silver. The thiosulfate leaching solution containing cadmium and silver thiosulfate complexes can potentially be used as a source of cadmium and silver [22,23]. This thiosulfate complex solution exhibits intense absorption in the ultraviolet (UV)-C region (200–280 nm). The photolysis of the cadmium and silver thiosulfate complexes has been previously studied [24,25]. However, the ultrasound-assisted photolysis of the cadmium and silver thiosulfate complex and the photocatalytic activity of the resulting CdS–Ag_2S have not been thoroughly investigated.

In this study, a novel UV photolysis co-precipitation method was applied to fabricate a CdS–Ag_2S photocatalyst from cadmium and silver poly-metallic thiosulfate complex solutions. Benefitting from the ion photochemical properties, the poly-metallic thiosulfate complex solution was obtained, which was then subsequently used to generate the CdS–Ag_2S nanocomposites. In dyeing wastewater, there are three representative pollutants, such as azo dyes, triphenylmethane dyes, and anthraquinone dyes. Among them, azo dyes account for 70–80%. Methyl orange (MO) is a typical azo dye with toxicity, stable chemical properties, and difficult biodegradation. The performance of CdS–Ag_2S was evaluated using the typical MO dye as a model compound, and the activity of the nanocomposites was investigated through the visible photocatalytic degradation of MO.

2 Methods

2.1 Reagents

Sodium thiosulfate ($Na_2S_2O_3$), cadmium chloride ($CdCl_2$), and silver nitrate ($AgNO_3$) used in the preparation of the simulated leaching solution were purchased from Sinopharm Chemical Reagent Co., Ltd. All the chemicals were of reagent grade. De-ionized (RO or UP) water prepared using a water purification machine was used both as a washing agent and as a solvent.

2.2 Procedure

The solution of the simulated Cd–Ag thiosulfate complexes solution was obtained by stoichiometrically mixing cadmium chloride ($CdCl_2$), silver nitrate ($AgNO_3$), and sodium thiosulfate ($Na_2S_2O_3$) in a stoichiometric manner, as explained below. The four steps in the CdS–Ag_2S composite preparation and testing are elaborated as follows: In Step 1, the simulated Cd–Ag thiosulfate complex solution (250 mL, Cd: 100 mg/L, and Ag: 10 mg/L) was produced in an Erlenmeyer flask through complexation reactions between the Cd^{2+}, Ag^{+}, and $S_2O_3^{2-}$ ions. In Step 2, the co-precipitation of CdS and Ag_2S was conducted using UV-C photolysis. Given a sufficient reaction time, cadmium and silver can co-precipitate completely in a 10:1 ratio. Thereafter, an ultrasound was used to enhance the dispersion of the suspension containing the CdS and Ag_2S precipitates. In Step 3, a centrifuge was used to separate the fabricated CdS–Ag_2S nanocomposites. In Step 4, the photocatalytic activity of the synthesized CdS–Ag_2S nanocomposites (25 mg) was examined *via* the degradation of MO (5 mg/L, 100 mL). Figure 1 shows a schematic diagram of the CdS–Ag_2S synthesis procedure.

2.3 Analytical methods

To further clarify the reaction mechanism, the UV decomposition rate of the cadmium/silver-thiosulfate complex was investigated in detail. Accordingly, the UV-induced

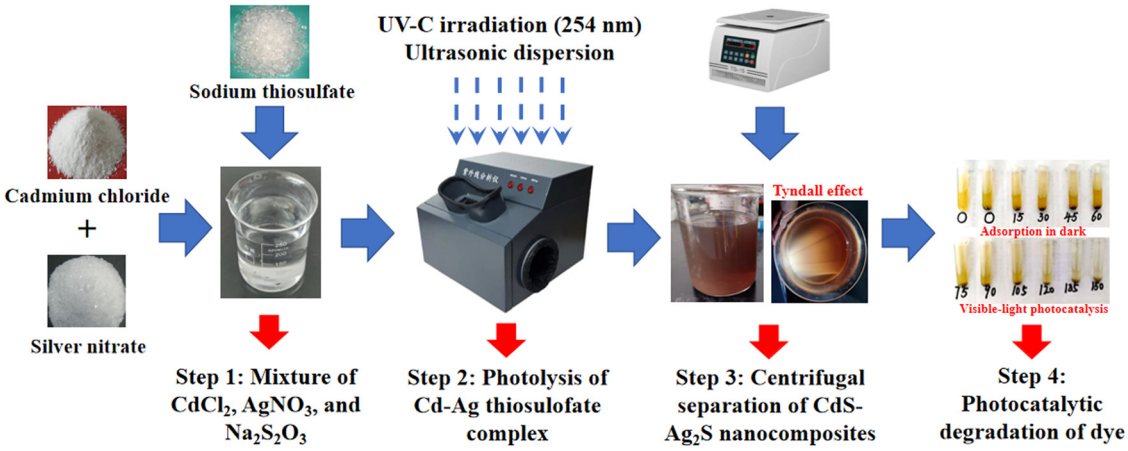

Figure 1: Schematic diagram of the CdS–Ag_2S synthesis method.

photolysis rate constant of the Cd–Ag thiosulfate complex was estimated. A Bruker D8 X-ray diffraction (XRD) was used to confirm the phase composition of the precipitate. The Highscore software was used to analyze XRD data with a standard card. The surface morphology of the CdS–Ag_2S nanocomposites was characterized using a JSM-5610LV SEM system. A Fourier transform infrared (FTIR) spectrophotometer (Perkin Elmer Spectrum 65) was also used to analyze the prepared sample. An Escalab 250xi XPS system was applied to study the composition and valence state of the elements on the precipitate surface. The analysis was conducted without sputtering or charge neutralization using monochromatic Al Kα X-radiation at a take-off angle of 90°. The C 1s line at 284.6 eV was used to calibrate the binding energies. The XPS Peak software was used to fit the XPS data, and the NIST XPS database was used to cross-check component information. A UV-2550 UV-Vis spectrometer was applied to obtain the UV-Vis DRS of the samples. The electrochemical properties of the samples were characterized by an electrochemical workstation. In the transient photocurrent study, light and dark experiments were performed every 20 s.

3 Results and discussions

3.1 Investigation of the UV photolysis precipitation

The thiosulfate leaching solution contains cadmium/silver-thiosulfate complex ions ($[CdAg_2(S_2O_3)_{2n}]^{4(n-1)-}$, $n = 1$ or 2), which are sources of metal and sulfur. A previous study demonstrated the ability of metal-thiosulfate to absorb UV energy and then decompose into metal sulfide. In this work, the UV photolysis mechanism that results in the formation of the cadmium/silver-thiosulfate complex was studied. The step-by-step details of the reaction mechanism are as follows: after absorbing energy from the UV-C (200–280 nm) radiation, the cadmium/silver-thiosulfate complex ions activate and enter an unstable excited state. The primary reaction of the photochemical process is described in equation (1). Subsequently, as shown in equation (2), the water molecule in the solution coordinates this activated Cd–Ag thiosulfate complex into the activated Cd–Ag hydroxide complex and thiosulfate ion. Finally, the activated Cd–Ag thiosulfate complex ions react with the activated state Cd–Ag hydroxide complex in the activated state to dissociate the S–S bond in the latter, resulting in the oxidation product of sulfate ions ($S_2O_3^{2-} \rightarrow SO_4^{2-}$) and reduction product of sulfur ions ($S_2O_3^{2-} \rightarrow S^{2-}$). A decrease in the solution pH was also observed owing to the formation of hydrogen ions – equations (2) and (3). Equations (2) and (3) represent the secondary reactions of the photochemical process, and equation (4) represents the overall reaction, which yields cadmium sulfide, silver sulfide, thiosulfate ions, sulfuric ions, and hydrogen ions.

$$[CdAg_2(S_2O_3)_{2n}]^{4(n-1)-} \xrightarrow{h\nu} \{[CdAg_2(S_2O_3)_{2n}]^{4(n-1)-}\}^{*} \{n = 1 \text{ or } 2\}, \quad (1)$$

$$\{[CdAg_2(S_2O_3)_{2n}]^{4(n-1)-}\}^{*} + 2nH_2O \xrightarrow{h\nu} \{[CdAg_2(OH)_{2n}]^{2(n-2)-}\}^{*} + 2nS_2O_3{}^{2-} + 2nH^{+} \{n = 1 \text{ or } 2\}, \quad (2)$$

$$[CdAg_2(S_2O_3)_{2n}]^{4(n-1)-} + \{[CdAg_2(S_2O_3)_{2n}]^{4(n-1)-}\}^{*} + \{[CdAg_2(OH)_{2n}]^{2(n-2)-}\}^{*} \xrightarrow{h\nu} 3CdS + 3Ag_2S + 6SO_4^{2-} + (4n - 6)S_2O_3^{2-} + (12 - 2n)H^{+} + (2n - 6)H_2O \{n = 1 \text{ or } 2\}, \quad (3)$$

$$[CdAg_2(S_2O_3)_{2n}]^{4(n-1)-} + 2H_2O \xrightarrow{hv} CdS + Ag_2S + 2SO_4^{2-} + (2n-2)S_2O_3^{2-} + 4H^+\{n = 1 \text{ or } 2\}. \quad (4)$$

To clarify the UV reaction mechanism, the photolysis rate constant of the Cd–Ag thiosulfate complex was investigated in this reaction together with the UV decomposition rate of the silver cadmium thiosulfate complex. Figure 2 shows the rate constant of the UV-C photolysis of various metal thiosulfate complexes. The photolysis rate constant of a pure Cd–thiosulfate complex (Cd: 80 mg/L) and an Ag–thiosulfate complex (Ag: 80 mg/L) was calculated as 0.00124 and 0.00622 min^{-1}, respectively. Additionally, the ratio of Cd to Ag in the synthesized nanocomposites depends on the decomposition rate of cadmium and silver. Furthermore, in the case of the cadmium–silver thiosulfate complex, the concentration of silver affects the decomposition rate of cadmium. When the concentration of cadmium was fixed (Cd = 80 mg/L), the rate at which cadmium decomposed decreased as the silver concentration increased. The rate constant of Cd photolysis in the Cd–Ag thiosulfate complex (Cd: 80 mg/L, Ag: 25 mg/L) was 0.00936 min^{-1}. This phenomenon can be explained by apparent rate constant (k_{obs}) calculation, which has been studied in the kinetics of Ag-thiosulfate photolysis, and the silver ion concentration is inversely proportional to the $k_{obs.}$ Similarly, when the concentration of cadmium is fixed in this work, the greater the concentration of silver ions, the greater the concentration of Cd–Ag thiosulfate complex ions generated, and the smaller the apparent rate constant.

3.2 Microstructure and chemical composition

To clearly illustrate the microstructure and chemical composition of CdS–Ag_2S nanocomposites, XRD, SEM, FT-IR, and XPS analyses were performed. XRD studies of pure CdS, pure Ag_2S, and photolyzed nanocomposites were conducted. The patterns obtained are shown in Figure 3. Three distinct broad peaks observed in the XRD pattern of the pure CdS (Figure 3b), at approximately 26.7°, 43.9°, and 51.8°, were also detected in the XRD pattern of the nanocomposites (Figure 3a), which are in accordance with the cadmium sulfide phase (PDF:00-002-0454). Similar to the XRD pattern of pure Ag_2S (Figure 3c), several peaks were observed in the nanocomposites (Figure 3a) spectrum at 20° and 80°, some of which are in accordance with peaks obtained from the Argentite phase (PDF:01-089-3840). The result demonstrates that cadmium and silver sulfides were predominantly precipitated *via* photolysis.

The surface morphology of the CdS–Ag_2S nanocomposites was observed by SEM, and the results are displayed in Figure 4. The precipitates have different shapes, uneven sizes, and poor dispersion and agglomeration. Owing to the limitations of SEM imaging, it is difficult to determine the exact particle size. However, the Tyndall effect observed for the prepared CdS–Ag_2S photocatalyst demonstrated that the particles of the product are in the nanoscale range.

FTIR spectra were collected in the range of 500–4,000 cm^{-1}. The spectra of the CdS–Ag_2S nanocomposites before and after photocatalysis are shown in Figure 5.

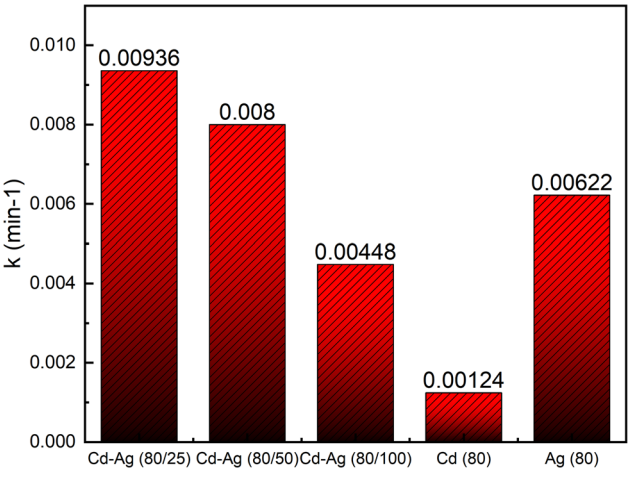

Figure 2: Rate constant (k) of photolysis of different M-thiosulfate by UV-C (Cd–Ag thiosulfate; Ag–thiosulfate; Cd–thiosulfate).

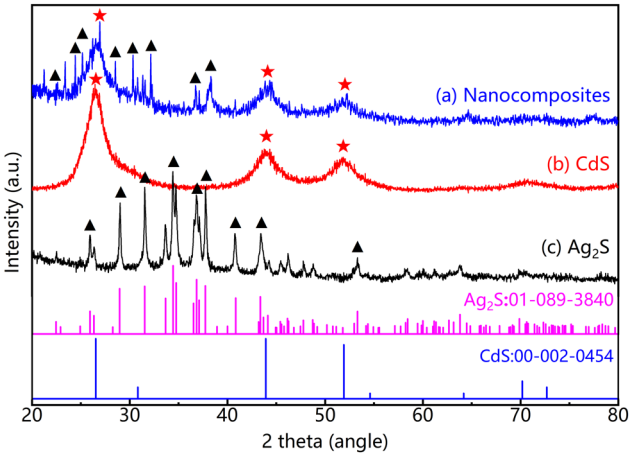

Figure 3: XRD patterns of different samples: (a) nanocomposites; (b) CdS; (c) Ag_2S.

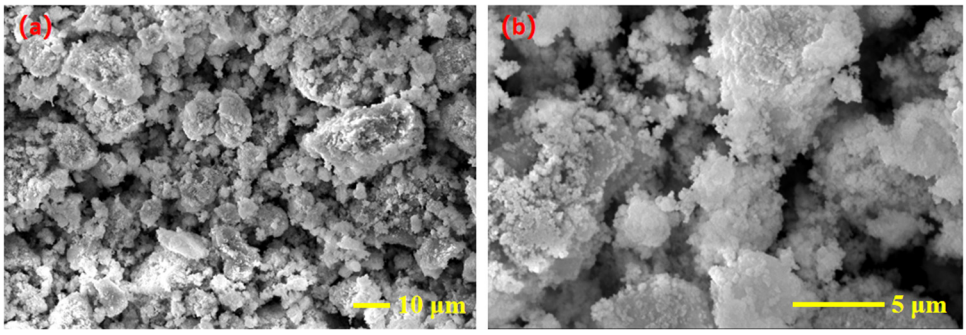

Figure 4: SEM images of the CdS–Ag_2S nanocomposite: (a) ×1,000; (b) ×5,000.

The absorption bands observed in the FTIR spectra at 3435.76 and 3435.96 cm^{-1} (Figure 5a and b) originate from the O–H group of the H_2O present on the surface of the nanocomposites. Figure 5(a) and (b) show absorption bands at 1002.63 and 1013.11 cm^{-1} that are attributed to sulfate, and the absorption bands at 1631.36 and 1630.66 cm^{-1} that are attributed to sulfoxide, indicating the presence of the S–O group [26]. Thus, the peaks at 666.01 cm^{-1} and 618.18 cm^{-1}, which are in the range of 500–750 cm^{-1}, are thus attributed to Ag–S and Cd–S metal-sulfur bonds [17]. No discernible difference was observed in the infrared spectra of the photocatalyst before and after photocatalysis, indicating the stability of the photocatalyst.

The CdS–Ag_2S nanocomposites prepared by photolysis were further analyzed using XPS to determine the valence state of the elements. As shown in Figure 6(a), Cd, Ag, and S were detected in the XPS survey scan. Figure 6(b) shows the XPS profile of Cd 3d, in which two broad peaks are observed. The first peak (411.3 eV) corresponds to Cd $3d_{3/2}$, and the second peak (405.0 eV) corresponds to Cd $3d_{5/2}$ [27,28]. The peaks of Cd 3d peaks were present at the binding energies of 405.0 eV and 411.3 eV. It can be concluded that Cd appeared as cadmium sulfide in the photoproduct, which agrees with the XRD results. Figure 6(c) shows the XPS profile of Ag-3d, in which two peaks with broad features were identified. Based on the NIST XPS database, the first peak (373.9 eV) corresponds to Ag $3d_{3/2}$, and the second peak (367.6 eV) corresponds to Ag $3d_{5/2}$ [29]. Therefore, it was verified that Ag appeared as silver sulfide in the photoproduct, which again agrees with the XRD results. The deconvoluted XPS S-2p spectrum displayed in Figure 6(d) shows two peaks in the narrowed bound energy scope. These S 2p peaks occur as doublets, namely S $2p_{3/2}$ and S $2p_{1/2}$. Makhova *et al.* [30] and Guo *et al.* [31,32] reported that the S 2p energy level of CdS and Ag_2S is at 161.5 and 161.0 eV, respectively. Duret-Thual *et al.* [33] reported that the S 2p energy level of $Na_2S_2O_3$ is at 162.4 eV, and the S 2p energy level of Na_2SO_4 is at 169.2 eV. It has also been reported that the S 2p energy level of SO_4^{2-} which comes from $CdSO_4$ or Ag_2SO_4 is at 168.0 eV. Therefore, according to the earlier analysis, the obtained nanocomposites primarily comprised cadmium sulfide and silver sulfide. These findings are supported by the XRD results displayed in Figure 3.

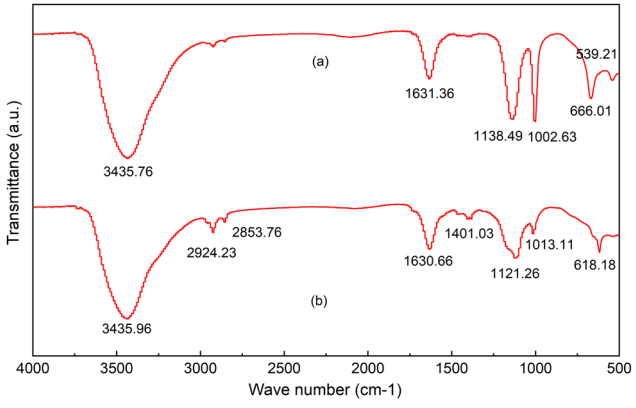

Figure 5: FTIR spectra of CdS–Ag_2S nanocomposite: (a) before photocatalysis; (b) after photocatalysis.

3.3 Optical and electrochemical properties

To clearly illustrate the optical and electrochemical properties of the CdS–Ag_2S nanocomposites, the UV–Vis DRS, transient photocurrent, and electrochemical impedance spectroscopy (EIS) were conducted, respectively. The UV–Vis DRS and corresponding bandgap energies were applied to scrupulously investigate the optical properties of the CdS–Ag_2S, Ag_2S, and CdS nanocomposites.

The UV–Vis spectra of the photolysis products are shown in Figure 7(a), where excellent absorption is observed in the range 200–1200 nm. The bandgap energies were

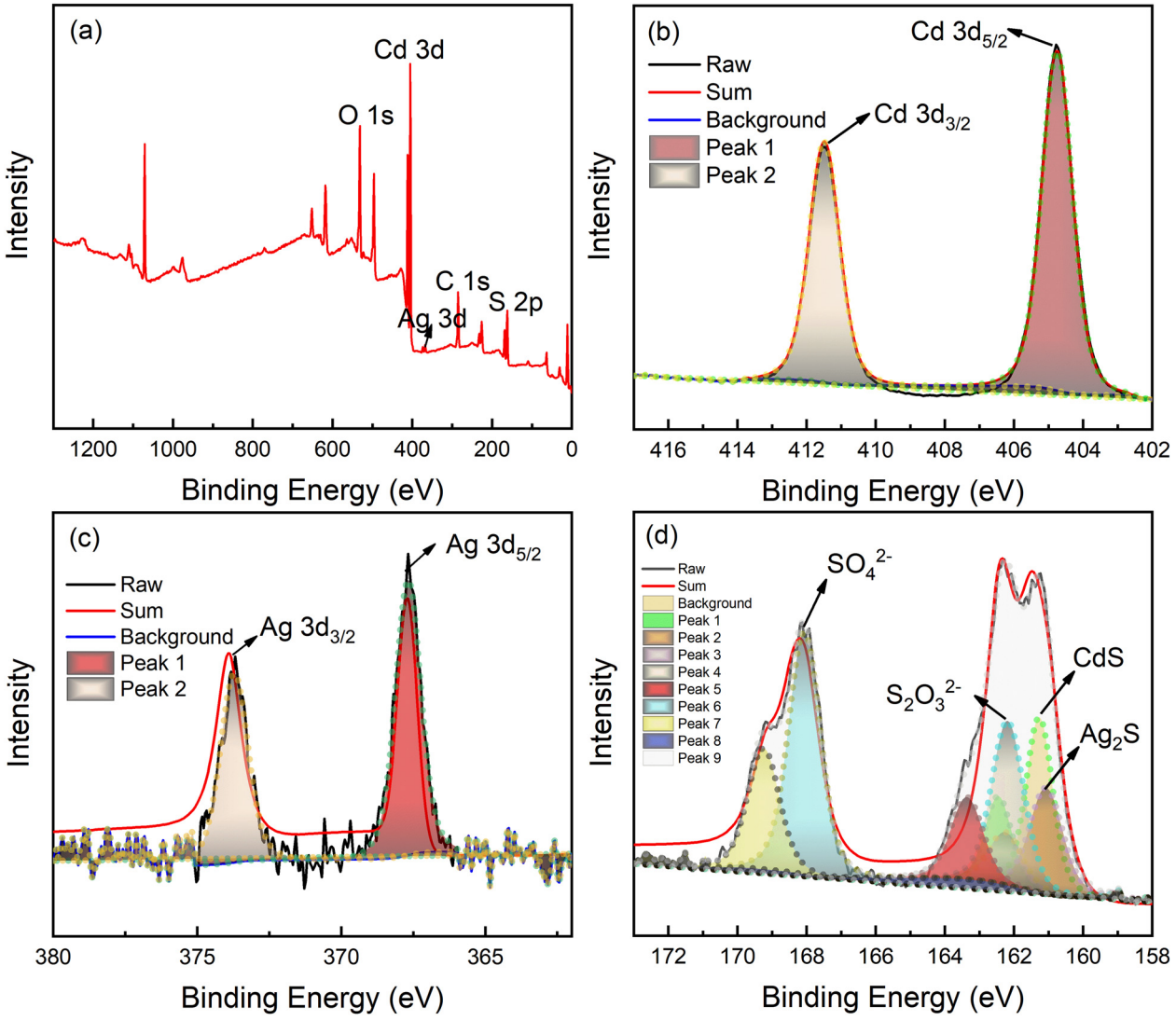

Figure 6: Deconvoluted XPS spectra for photoproduct: (a) survey spectrum; (b) Cd-3d spectrum; (c) Ag-3d spectrum; (d) S-2p spectrum.

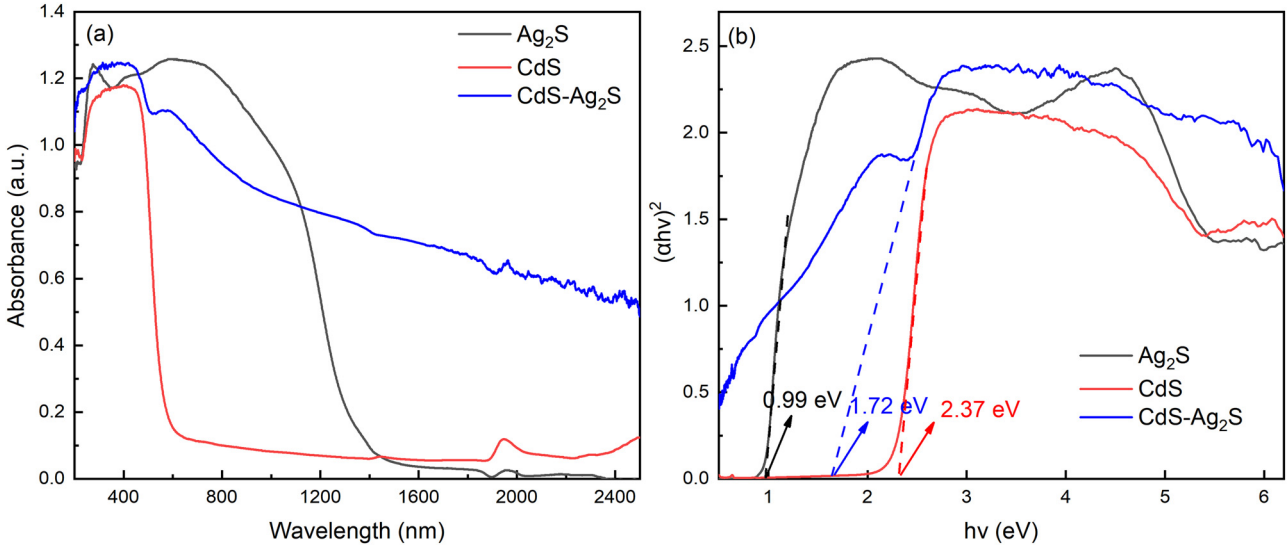

Figure 7: (a) UV-Vis absorbance spectra of Ag_2S, CdS, and CdS–Ag_2S; (b) plots of $(\alpha h\nu)^2$ *versus* energy ($h\nu$) of Ag_2S, CdS, and CdS–Ag_2S.

estimated using a plot of $(\alpha h\nu)^2$ *versus* photo energy ($h\nu$). The intercept of the tangent to this plot provides a good approximation of the indirect bandgap energy. The apparent bandgap can be calculated using the Kubelka–Munk formula, as shown in equation (5).

$$(\alpha h\nu)^2 = A(h\nu - E_g), \tag{5}$$

where α, h, ν, A, and E_g represent the absorbance coefficient, Plank's constant, incident photon frequency, absorbance, and apparent bandgap, respectively. Figure 7(b) shows that this curve forms the converted Kubelka–Munk formula curve. The intersection of the curve's tangent and abscissa determines the apparent bandgap energy. Accordingly, the estimated bandgap energies for Ag_2S, CdS, and CdS–Ag_2S, are 0.99, 2.37, and 1.72 eV, respectively. The first two values are in accordance with the theoretical values of silver sulfide and cadmium sulfide. The design and development of CdS–Ag_2S is to reduce the bandgap and enhance visible light absorption by introducing silver components to adjust the position of valence band (VB) or conduction band (CB), and exhibits better photocatalytic activity.

The transient photocurrent was measured using electrochemical workstations to monitor the migration of photogenerated carriers in the nanocomposites. Figure 8(a) displays the transient photocurrent spectra of the cadmium/silver sulfide prepared *via* ultrasound-assisted UV photolysis, and cadmium/silver sulfide and cadmium sulfide nanocomposites prepared *via* UV photolysis. The analysis showed that the current value was observed to increase every 20 s of irradiation time, but when blocked, it rapidly decreased in the subsequent 20 s interval. This indicates that the photogenerated charge carriers were transferred to the electrode, thereby generating a photocurrent. Compared with the CdS–Ag_2S nanocomposites prepared by UV photolysis, the I–t curves of cadmium/silver sulfide synthesized through ultrasound-assisted UV photolysis produced a higher current every 20 s. This demonstrates that the ultrasound treatment improves the dispersion and strengthens the photocatalytic activity. Compared with pure CdS nanocomposites synthesized *via* pure UV photolysis, the I–t curves of the previously mentioned cadmium/silver sulfide prepared *via* ultrasound-assisted UV photolysis generated approximately the same or a slightly lower current at every 20 s. This demonstrates that a higher photocurrent improves light absorption and electron extraction, which are in turn beneficial for charge separation [34]. The CdS–Ag_2S EIS Nyquist plots of CdS–Ag_2S are presented in Figure 8(b). The arc radius of CdS–Ag_2S with ultrasound-assisted UV photolysis (presented by the blue line) is smaller than that of CdS–Ag_2S without ultrasound (presented by the red line), indicating that the ultrasound can enhance the charge transfer resistance and the interfacial charge separation. However, the arc radius of CdS–Ag_2S (ultrasound-assisted UV photolysis) is bigger than that of pure CdS (UV-photolysis, black line), which is consistent with the I–t curves.

3.4 Visible light photocatalysis activity of CdS–Ag_2S nanocomposites

Microstructure, chemical composition, optical, and electrochemical properties of the CdS–Ag_2S nanocomposites were compared with the photocatalytic activity of CdS–Ag_2S nanocomposites and pure CdS which are prepared by

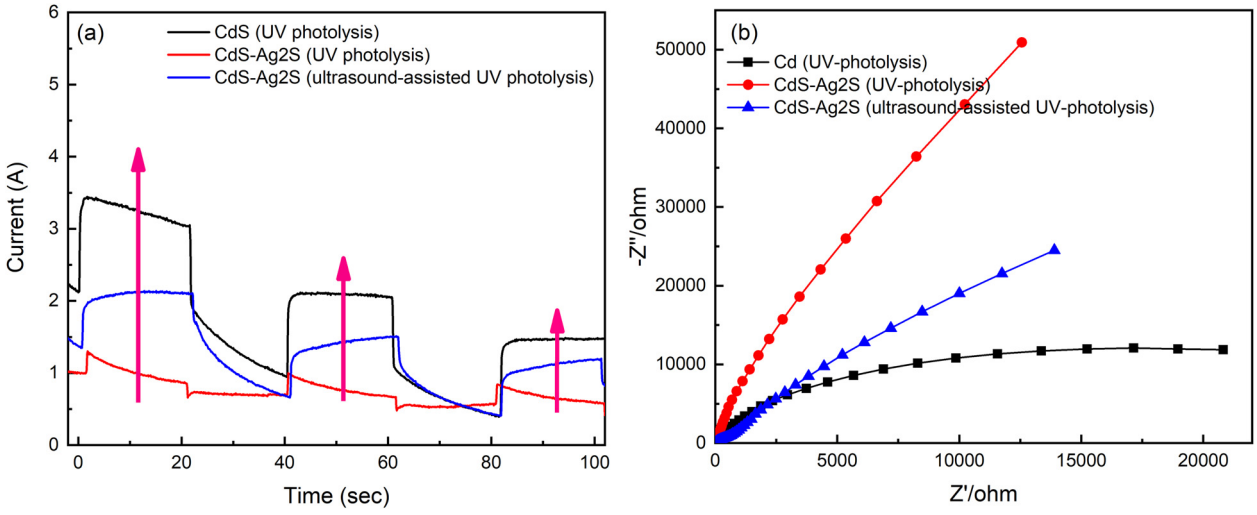

Figure 8: (a) Transient photocurrent (I–t curves); (b) electrochemical Impedance Spectroscopy (EIS) of different samples.

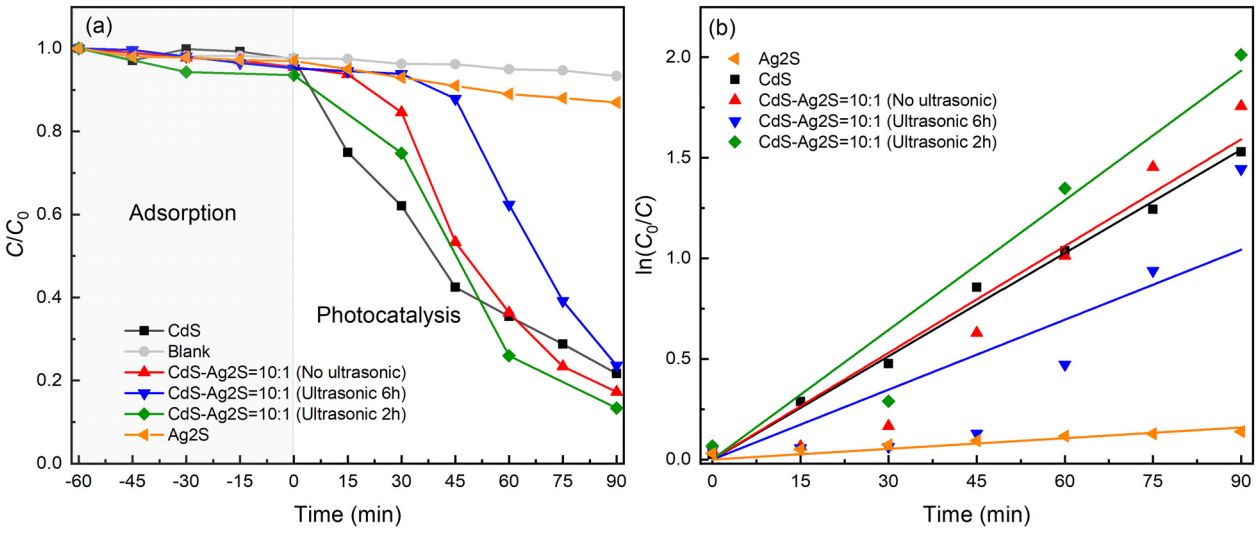

Figure 9: Time-course variation of C/C_0 toward MO: (a) C/C_0 *vs* time; (b) $\ln(C_0/C)$ *vs* time.

ultrasound-assisted UV photolysis in the photodegradation of MO under visible light irradiation. The degree of degradation was measured by the characteristic absorption wavelength of 465 nm, and the C/C_0 *vs* irradiation time is plotted in Figure 9. In the photocatalytic activity analysis, the adsorption (−60 to 0 min) and the C/C_0 ratio remained constant, indicating that the MO can hardly adsorb on the surface of the CdS–Ag_2S nanocomposite. During photocatalysis (0 to 90 min), the C/C_0 of the blank experiment remained constant, indicating that the MO solutions do not exhibit self-degradation. The C/C_0 of CdS–Ag_2S nanocomposites decreased with time, but it increased under conditions of ultrasonication for 6 h, no ultrasonication, and ultrasonication for 2 h after 90 min. It possessed a photocatalytic efficiency of 87% after 90 min under the condition of ultrasonication for 2 h, which is higher than that of pure CdS with 78% at the same time. The rate constant of the CdS–Ag_2S nanocomposites under different conditions, namely ultrasonication for 6 h, no ultrasonication, and ultrasonication for 2 h, was calculated to be 0.01159, 0.01769, and 0.02148 min^{-1}, respectively. The sample ultrasonicated for 2 h with UV photolysis exhibits a fine degradation rate because the ultrasound can contribute to the dispersion of the system and facilitate the formation of nanocomposites. However, a longer ultrasonic treatment time may damage the structure, causing a decrease in the reaction rate. To objectively evaluate the photocatalytic effect of the nanocomposites prepared by this method, and the capabilities of different

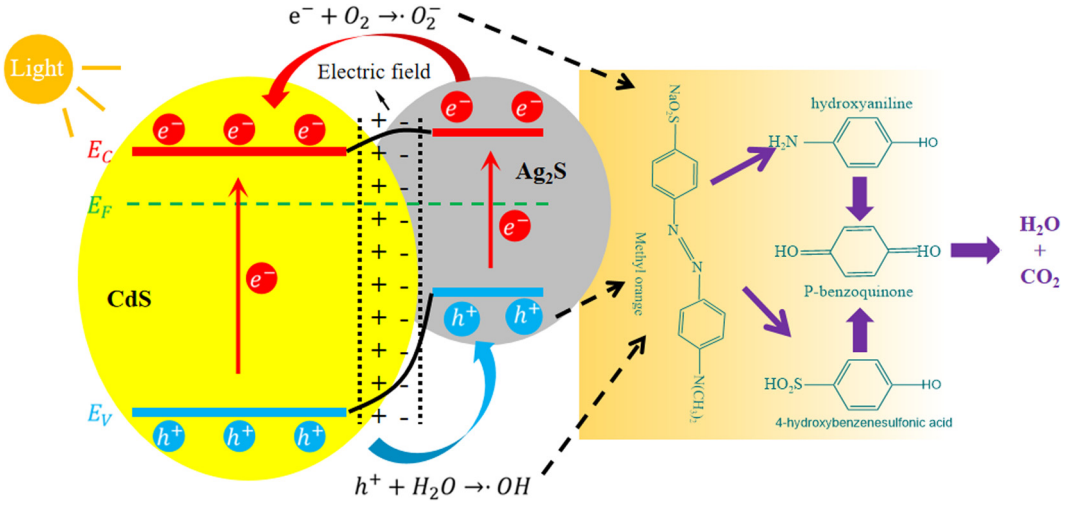

Figure 10: Degradation mechanism of MO by CdS–Ag_2S nanocomposites under visible light irradiation.

components were examined. The results show that the catalytic effect of Ag_2S is very poor, and the rate constant of the pure Ag_2S nanocomposites with UV photolysis was 0.00177 min^{-1}. The rate constant of the pure CdS nanocomposites with UV photolysis was 0.01711 min^{-1}. The rate constant of the synthesized CdS–Ag_2S nanocomposites with UV photolysis was increased to 0.02148 min^{-1} with the formation of the CdS–Ag_2S nanocomposites, indicating that the ultrasound-assisted UV photolysis method can produce nanocomposites with better properties.

The photocatalytic mechanism of the degradation of MO by CdS–Ag_2S nanocomposites is shown in Figure 10. Under visible light irradiation, CdS undergoes electron band-to-band transition, and electrons (e^-) transition from valence band (VB) to conduction band (CB), forming photogenerated electron–hole pairs (e^-/h^+). Photogenerated electron–hole pairs (e^-/h^+) have strong oxidation and reduction properties. The electrons (e^-) on the conduction band (CB) reduce oxygen to superoxide anion ($^{\bullet}O_2^-$), and the holes (h^+) on the valence band (VB) oxidize water (H_2O) to hydroxyl radical ($^{\bullet}OH$), generating active oxidizing substances. However, there are defects on the surface of CdS, resulting in the recombination of photogenerated carriers. The CdS–Ag_2S nanocomposite is adopted. The edge potentials of the valence band (VB) and conduction band (CB) of Ag_2S are higher than those of CdS. The electrons (e^-) on the conduction band (CB) of Ag_2S are transferred to the conduction band (CB) of CdS, and the holes (h^+) on the valence band (VB) of CdS are transferred to the valence band (VB) of Ag_2S, thus realizing the effective separation of carriers, promoting the degradation of MO to water and carbon dioxide, and improving the photocatalytic activity [35,36].

4 Conclusions

In this study, a novel method for synthesizing CdS–Ag_2S nanocomposites from complex solutions is presented. The photochemical co-precipitation of the Cd–Ag thiosulfate complex (Cd: 100 mg/L; Ag: 10 mg/L) produced the CdS–Ag_2S nanocomposites. The XRD and XPS results confirmed that the nanocomposites are chemically composed of CdS and Ag_2S. Based on the Tyndall effect, the size of the CdS–Ag_2S particles is considered to be in the nanoscale. The DRS result indicated that the bandgap energy of CdS–Ag_2S is 1.72 eV. Investigations into the visible-light photocatalytic activity of the CdS–Ag_2S nanocomposites using the *I–t* curves demonstrated that they can produce a photocurrent under the conditions of stimulated solar irradiation. Investigations into the photocatalytic degradation of MO using the as-synthesized samples revealed that the CdS–Ag_2S nanocomposite possessed a photocatalytic efficiency of 87% after 90 min. According to the kinetic study, which showed that the first-order equation can fit the data, the use of the proposed ultrasound-assisted UV photolysis method can yield nanocomposites with good photocatalytic performance, and the rate constant for the CdS–Ag_2S nanocomposites obtained using this method is 0.02148 min^{-1}.

Funding information: This project was supported by the National Natural Science Foundation of China (Grant No. 52104349), and China Postdoctoral Science Foundation (Grant No. 2021M690915). This project was also funded by The Key Technologies R&D Program of Henan Province (Grant No. 222102320435), and The Key Scientific Research Project of Colleges and Universities in Henan Province (Grant No. 21A450001).

Author contributions: All authors have accepted responsibility for the entire content of this manuscript and approved its submission.

Conflict of interest: The authors state no conflict of interest.

References

[1] Huang J, Luo Y, Weng M, Yu J, Sun L, Zeng H, et al. Advances and applications of phase change materials (PCMs) and PCMs-based technologies. ES Mater Manuf. 2021;13:23–39.

[2] Kadam AN, Salunkhe TT, Kim H, Lee SW. Biogenic synthesis of mesoporous N–S–C tri-doped TiO_2 photocatalyst *via* ultrasonic-assisted derivatization of biotemplate from expired egg white protein. Appl Surf Sci. 2020;518:146194.

[3] Mukhopadhyay A, Tripathy BK, Debnath A, Kumar M. Enhanced persulfate activated sono-catalytic degradation of brilliant green dye by magnetic $CaFe_2O_4$ nanoparticles: Degradation pathway study, assessment of bio-toxicity and cost analysis. Surf Interfaces. 2021;26:101412.

[4] Bose S, Tripathy BK, Debnath A, Kumar M. Boosted sono-oxidative catalytic degradation of Brilliant green dye by magnetic $MgFe_2O_4$ catalyst: Degradation mechanism, assessment of bio-toxicity and cost analysis. Ultrason Sonochem. 2021;75:105592.

[5] Tripathy BK, Kumar S, Kumar M, Debnath A. Microwave induced catalytic treatment of brilliant green dye with carbon doped zinc oxide nanoparticles: Central composite design, toxicity assessment and cost analysis. Environ Nanotechnol Monit Manag. 2020;14:100361.

[6] Liexiao L, Xiaofeng S, Tao X, Huajing G, Shifa W, Zao Y, et al. Template-free synthesis of $Bi_2O_2CO_3$ hierarchical nanotubes self-assembled from ordered nanoplates for promising

photocatalytic applications. Phys Chem Chem Phys. 2022;24:8279–95.
[7] Supekar A, Kapadnis R, Bansode S, Bhujbal P, Kale S, Jadkar S, et al. Cadmium telluride/cadmium sulfide thin films solar cells:a review. ES Energy Environ. 2020;10:3–12.
[8] Rahane GK, Jathar SB, Rondiya SR, Jadhav YA, Barma SV, Rokade A, et al. Photoelectrochemical investigation on the cadmium sulfide (CdS) thin films prepared using spin coating technique. ES Mater Manuf. 2020;11:57–64.
[9] Zhao Y, Li L, Zuo Y, He G, Chen Q, Meng Q, et al. Reduced graphene oxide supported ZnO/CdS heterojunction enhances photocatalytic removal efficiency of hexavalent chromium from aqueous solution. Chemosphere. 2022;286:131738.
[10] Li LL, Yin XL, Sun YQ. Facile synthesized low-cost MoS_2/CdS nanodots-on nanorods heterostructures for highly efficient pollution degradation under visible light irradiation. Sep Purif Technol. 2019;212:135–41.
[11] Lv T, Li D, Hong Y, Luo B, Xu D, Chen M, et al. Facile synthesis of CdS/$Bi_4V_2O_{11}$ photocatalysts with enhanced visible-light photocatalytic activity for degradation of organic pollutants in water. Dalton Trans. 2017;46:12675–82.
[12] Liu YP, Shen SJ, Zhang JT, Zhong WW, Huang XH. Cu_2xSe/CdS composite photocatalyst with enhanced visible light photocatalysis activity. Appl Surf Sci. 2019;478:762–9.
[13] Tingting C, Huajing G, Guorong L, Zhongsheng P, Shifa W, Zao Y, et al. Preparation of core-shell heterojunction photocatalysts by coating CdS nanoparticles onto $Bi_4Ti_3O_{12}$ hierarchical microspheres and their photocatalytic removal of organic pollutants and Cr(VI) ions. Colloids Surf A: Physicochem Eng Aspects. 2022;633:127918.
[14] Yi Z, Ye J, Kikugawa N, Kako T, Ouyang S, Stuart-Williams H, et al. An orthophosphate semiconductor with photooxidation properties under visible-light irradiation. Nat Mater. 2010;9(7):559–64.
[15] Lu HD, Wang JX, Du ZY, Liu YP, Li M, Chen P, et al. In-situ anionexchange synthesis AgCl/$AgVO_3$ hybrid nanoribbons with highly photocatalytic activity. Mater Lett. 2015;157:231–4.
[16] Wang C, Zhai J, Jiang H, Liu D, Zhang L. CdS/Ag_2S nanocomposites photocatalyst with enhanced visible light photocatalysis activity. Solid State Sci. 2019;98:106020.
[17] Iqbal T, Ali F, Khalid NR, Bilal Tahir M, Ijaz M. Facile synthesis and antimicrobial activity of CdS-Ag_2S nanocomposites. Bioorganic Chem. 2019;90:103064.
[18] Han G, Jin YH, Burgess RA, Dickenson NE, Cao XM, Sun Y. Visible-lightdriven valorization of biomass intermediates integrated with H_2 production catalyzed by ultrathin Ni/CdS nanosheets. J Am Chem Soc. 2017;139:15584–7.
[19] Di T, Cheng B, Ho W, Yu J, Hua T. Hierarchically CdS-Ag_2S nanocomposites for efficient photocatalytic H_2 production. Appl Surf Sci. 2019;470:196–204.
[20] El-Nahass MM, Farag AA, Ibrahim EM, Abd-El-Rahman S. Structural, optical and electrical properties of thermally evaporated Ag_2S thin films. Vacuum. 2004;72(4):453–60.
[21] Abd-Elkader OH, Shaltout AA. Characterization and antibacterial capabilities of nanocrystalline CdS thin films prepared by chemical bath deposition. Mater Sci Semicond Process. 2015;35:132–8.
[22] Sebastián G, Karla G, Ernestode LT, Alicia G. Precious metals recovery from waste printed circuit boards using thiosulfate leaching and ion exchange resin. Hydrometallurgy. 2019;186:1–11.
[23] Wang P, Cheng H, Ding J, Ma J, Jiang J, Huang Z, et al. Cadmium removal with thiosulfate/permanganate (TS/Mn(VII)) system: MnO_2 adsorption and/or CdS formation. Chem Eng J. 2020;380:122585.
[24] Egorov NB, Eremin LP, Larionov AM, Usov VF, Tsepenko EA, D'yachenko AS. Products of photolysis of cadmium thiosulfate aqueous solutions. High Energy Chem. 2008;42:119–22.
[25] Han C, Wang G, Cheng C, Shi C, Yang Y, Zou M. A kinetic and mechanism study of silver-thiosulfate complex photolysis by UV-C irradiation. Hydrometallurgy. 2020;191:105212.
[26] Zamiri R, Abbastabar Ahangar H, Zakaria A, Zamiri G, Shabani M, Singh B, Ferreira JM. The structural and optical constants of Ag_2S semiconductor nanostructure in the Far-Infrared. Chem Cent J. 2015;9(1):28.
[27] Di T, Zhu B, Zhang J, Cheng B, Yu J. Enhanced photocatalytic H_2 production on CdS nanorod using cobalt-phosphate as oxidation cocatalyst. Appl Surf Sci. 2016;389:775–82.
[28] Yu W, Zhang S, Chen J, Xia P, Richter MH, Chen L, et al. Biomimetic Z-scheme photocatalyst with a tandem solid-state electron flflow catalyzing H_2 evolution. J Mater Chem A. 2018;6:15668–74.
[29] An C, Wang J, Jiang W, Zhang M, Ming X, Wang S, et al. Strongly visiblelight responsive plasmonic shaped AgX: Ag (X = Cl, Br) nanoparticles for reduction of CO_2 to methanol. Nanoscale. 2012;4:5646–50.
[30] Makhova L, Mikhlin Y, Romanchenko A. A combined XPS, XANES and STM/STS study of gold and silver deposition on metal sulphides. Nucl Instrum Methods Phys Res Sect A: Accel Spectrometers Detect Assoc Equip. 2007;575:75–7.
[31] Guo J, Liang Y, Liu L, Hu J, Wang H, An W, et al. Core-shell structure of sulphur vacancies-CdS@CuS: Enhanced photocatalytic hydrogen generation activity based on photoinduced interfacial charge transfer. J Colloid Interf Sci. 2021;600:138–49.
[32] Zhang X, Li N, Wu J, Zheng Y, Tao X. Defect-rich O-incorporated 1TMoS_2 nanosheets for remarkably enhanced visible-light photocatalytic H_2 evolution over CdS: The impact of enriched defects. Appl Catal B. 2018;229:227–36.
[33] Duret-Thual C, Costa D, Yang WP, Marcus P. The role of thiosulfates in the pitting corrosion of Fe-17Cr alloys in neutral chloride solution: Electrochemical and XPS study. Corros Sci. 1997;39(5):913–33.
[34] Yu J, Jin J, Cheng B, Jaroniec M. A noble metal-free reduced graphene oxide–CdS nanorod composite for the enhanced visible-light photocatalytic reduction of CO_2 to solar fuel. J Mater Chem A. 2014;2:3407–16.
[35] Lee J, Lee Y, Bathula C, Kadam AN, Lee SW. A zero-dimensional/two-dimensional Ag-Ag_2S-CdS plasmonic nanohybrid for rapid photodegradation of organic pollutant by solar light. Chemosphere. 2022;296:133973.
[36] Okla M, Janani B, AL-ghamdi AA, Abdel-Maksoud MA, AbdElgawad H, Das A, et al. Facile construction of 3D CdS-Ag_2S nanospheres: A combined study of visible light responsive phtotocatalysis, antibacterial and anti-biofilm activity. Colloids Surf A: Physicochem Eng Aspects. 2022;632:127729.